Journal of Solid Mechanics Vol. 2, No. 4 (2010) pp. 316-331

Stress Analysis of Two-directional FGM Moderately Thick Constrained Circular Plates with Non-uniform Load and Substrate Stiffness Distributions

M.M. Alipour, M. Shariyat*

Faculty of Mechanical Engineering, K.N. Toosi University of Technology, Tehran 19991-43344, Iran

Received 4 October 2010; accepted 10 November 2010

ABSTRACT

In the present paper, bending and stress analyses of two-directional functionally graded (FG) circular plates resting on non-uniform two-parameter foundations (Winkler-Pasternak foundations) are investigated using a first-order shear-deformation theory. To enhance the accuracy of the results, the transverse stress components are derived based on the three dimensional theory of elasticity. The solution is obtained by employing the differential transform method (DTM). The material properties are assumed to vary in both transverse and radial directions according to power and exponential laws, respectively. Intensity of the transverse load is considered to vary according to a second-order polynomial. The performed convergence analysis and the comparative studies demonstrate the high accuracy and high convergence rate of the approach. A sensitivity analysis consisting of evaluating effects of different parameters (e.g., exponents of the material properties, thickness to radius ratio, trend of variations of the foundation stiffness, and edge conditions) is carried out. Results reveal that in contrast to the available constitutive-law-based solutions, present solution guarantees continuity of the transverse stresses at the interfaces between layers and may also be used for stress analysis of the sandwich panels. The results are reported for the first time and are discussed in detail.

Keywords: Bending stress analysis; three-dimensional theory of elasticity; two-directional functionally graded materials; circular plates; elastic foundation; differential transform method.

1 INTRODUCTION

THE necessity of monitoring the local variations of the material properties in the whole component to meet the design requirements and achieving continuous stress distributions and optimized designs has led to creation of various functionally graded materials (FGMs). Therefore, depending on the function of the component, it is possible to utilize one-, two- or three-directional functionally graded materials. Examples of functionally graded circular plates resting on two-parameter (Winkler-Pasternak) elastic foundations may be found in aerospace, civil, mechanical, nuclear and offshore applications. Driven plate of a friction clutch is an example of the mentioned plates. There are two approaches for designing this typical component: the constant-life and constant-pressure approaches. Therefore, the distributed forces exerted by the foundation may not be uniform even for a uniform displacement field. Subsequently, as a general case, the stiffness of the foundation may not be uniform.

Some researchers have investigated bending of the functionally graded plates employing the plate theories. Axisymmetric bending and stretching of the functionally graded solid and annular circular plates was studied by

* Corresponding author. Tel.: +98 9122727199; Fax: +98 21 88674748.
E-mail address: m_shariyat@yahoo.com, shariyat@kntu.ac.ir (M. Shariyat).

Reddy et al. [1] using the first-order shear-deformation Mindlin plate theory. Ma and Wang [2] employed the third-order shear-deformation plate theory to study axisymmetric bending of the functionally graded circular plates. Saidi et al. [3] and Sahraee and Saidi [4] studied axisymmetric bending and stretching of functionally graded (FG) circular plates subjected to uniform transverse loadings based on the higher-order shear-deformation plate theories. An analytical solution based on the first-order shear-deformation plate theory approach was presented by Jomehzadeh et al. [5] for bending analysis of the functionally graded annular sector plates. Golmakani and Kadkhodayan [6] studied axisymmetric nonlinear bending of an annular functionally graded plate using the dynamic relaxation method combined with the finite difference technique.

It is evident that results of the three-dimensional theory of elasticity are exact and more accurate than the plate theories which are two-dimensional theories whose dependency on the transverse coordinate is prescribed. Assuming the material properties to vary according to an exponential law in both transverse and radial directions, Nie and Zhong [7] investigated axisymmetric bending of the two-directional functionally graded circular and annular plates based on the three-dimensional theory of elasticity. Li et al. [8] obtained an elasticity solution for axisymmetric bending of FGM circular and annular plates subject to polynomial loads of even order. The problem of a functionally graded, transversely isotropic, magneto–electro-elastic circular plate acted on by a uniform load was treated by Li et al. [9] based on the three-dimensional theory of elasticity. Yang et al. [10] presented an analytical solution for bending of annular plates under uniform loadings. Lei and Zheng [11] presented an exact solution for axisymmetric bending of functionally graded circular plates under elastically supported and rigid slipping edge conditions. Based on the three-dimensional theory of elasticity, Yun et al. [12] investigated axisymmetric bending of functionally graded circular plates subject to Bessel function-type transverse loads using the direct displacement method. Nie and Zhong [13] investigated the dynamic behavior of the two-directional FGM annular plates based on the three-dimensional theory of elasticity using the state-space method combined with the one dimensional differential-quadrature method (DQM). Sepahi et al. [14] used the DQ method for analysis of axisymmetric large deflection response of a simply supported annular FGM plate resting on a three-parameter elastic foundation. Sburlati and Bardella [15] obtained three-dimensional elastic solutions for a functionally graded thick circular plate subjected to axisymmetric conditions.

Reviewing the literature reveals that very limited papers have been published on the two-directional functionally graded circular plates [7, 13, 16-17]. Bending and stress analysis of two-directional functionally graded circular plates resting on elastic foundations has not been performed before, especially for non-uniform load and foundation stiffness distributions. Present research is devoted to bending and stress analysis of two-directional functionally graded circular plates resting on non-uniform two-parameter Winkler-Pasternak elastic foundations. The material properties are assumed to be graded in the transverse and radial directions according to power and exponential laws, respectively. The governing equations are derived based on Mindlin's plate theory in conjunction with the three dimensional theory of elasticity. A semi-analytical method based on the differential transform method (DTM) is employed to extract the semi-analytical solution. Some of the most significant novelties of the paper are: (i) performing bending and stress analyses of the two-directional functionally graded circular plates for the first time, (ii) in contrast to the traditional constitutive-equation-based first-order shear deformation theories, results are modified using the three-dimensional theory of elasticity and subsequently, (iii) the solution may also be used for analyzing the sandwich plates due to a priori satisfying the continuity conditions of the transverse stress components, and (iv) present results are accurate enough even for the thick plates.

2 GOVERNING EQUATIONS OF MOTION OF THE CIRCULAR PLATE

Consider a circular plate made of a two-directional functionally graded material (FGM) and subjected to both non-uniform load and non-uniform foundation stiffness distributions, as shown in Fig. 1. Based on Mindlin-Reissner plate theory, displacement field of the plate may be described as follows [18]:

$$u = u_0 + z\psi_r, \qquad w = w_0 \tag{1}$$

where the symbol "," stands for the partial derivative, u_0 and w_0 are respectively the radial and transverse displacement components of the reference layer (e.g. the mid-surface) of the circular plate, and the coordinate z is measured from the reference layer and is positive upward. ψ_r is rotation of the normal to reference layer. For small deflections, the strain-displacement relations may be written as [18]:

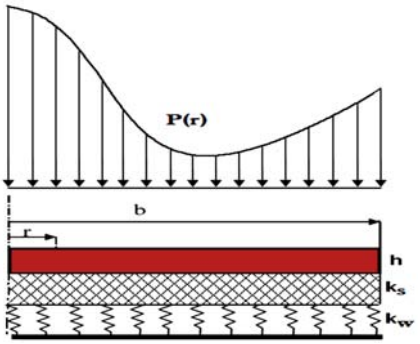

Fig. 1
Geometry and foundation parameters of the two-directional functionally graded circular plate.

$$\varepsilon_r = u_{,r} \quad \varepsilon_\theta = \frac{u}{r}, \quad \varepsilon_{rz} = u_{,z} + w_{,r} \tag{2}$$

On the other hand, as a consequence of assumptions of Mindlin-Reissner plate theory, Hooke's generalized stress-strain law may be expressed as [18]:

$$\sigma_r = \frac{E}{1-\nu^2}(\varepsilon_r + \nu\varepsilon_\theta), \quad \sigma_\theta = \frac{E}{1-\nu^2}(\varepsilon_\theta + \nu\varepsilon_r), \quad \sigma_{rz} = \kappa^2 \frac{E}{2(1+\nu)}\varepsilon_{rz} \tag{3}$$

where E and ν are modulus of elasticity and Poisson's ratio, respectively and κ^2 denotes the transverse shear correction factor which is usually introduced in the first-order shear-deformation plate/shell theories (FSDT) in order to correct the transverse shear rigidities of the plate. In the present analysis, this coefficient is adopted as $\kappa^2 = (\pi^2/12)$.

Assuming the constituent materials of the FGM plate to be ceramic and metal, variations of a representative material property p in the transverse and radial directions may be assumed to be [19]:

$$p = (p_c V_c + p_m V_m) e^{\phi r} \tag{4}$$

In which the subscripts c and m refer to ceramic and metal, respectively. V_c and V_m, the volume fractions of the ceramic and metal materials, may be related as follows [19]:

$$V_c + V_m = 1 \tag{5}$$

The metal volume fraction is assumed to follow a power-law distribution in the transverse direction [19]:

$$V_m = \left(\frac{1}{2} - \frac{z}{h}\right)^g \tag{6}$$

where g is the positive definite power–law index. From Eqs. (4-6), variations of the modulus of elasticity of the FG plate may be given by:

$$E(z,r) = [(E_m - E_c)V_m + E_c] e^{\frac{r}{b}\mu} \tag{7}$$

The governing equations of motion may be derived by using principle of minimum total potential energy. Employing this principle leads to the following three governing equations for the plate in the cylindrical coordinate system (r, θ, z) [2]:

$$N_{r,r}+\frac{N_r-N_\theta}{r}=0 \tag{8a}$$

$$M_{r,r}+\frac{1}{r}(M_r-M_\theta)-Q_r=0 \tag{8b}$$

$$Q_{r,r}+\frac{1}{r}Q_r=P+k_w(1+\alpha r+\beta r^2)w-k_s\left(w,_{rr}+\frac{1}{r}w,_r\right) \tag{8c}$$

where the intensity of the transversely distributed load is considered to vary according to a general second-order polynomial

$$P=P_0(\lambda+\gamma r+\xi r^2) \tag{9}$$

and the stress resultants M_i, N_i, Q_i (i=r, θ) are

$$\begin{Bmatrix}M_r\\M_\theta\end{Bmatrix}=\int_{-h/2}^{h/2}\begin{Bmatrix}\sigma_r\\\sigma_\theta\end{Bmatrix}z\ \mathrm{d}z,\qquad \begin{Bmatrix}N_r\\N_\theta\end{Bmatrix}=\int_{-h/2}^{h/2}\begin{Bmatrix}\sigma_r\\\sigma_\theta\end{Bmatrix}\mathrm{d}z,\qquad Q_r=\int_{-h/2}^{h/2}\sigma_{rz}\ \mathrm{d}z \tag{10}$$

In Eq. (8c), it is implicitly assumed that Winkler's stiffness of the Winkler-Pasternak-type elastic substrate varies in the radial direction according to a second-order polynomial. Based on Eqs. (1-3, 7, 8, and 10), one may write:

$$\begin{aligned}
M_r&=B(r)\left(u_{0,r}+\nu\frac{u_0}{r}\right)+D(r)\left(\psi_r,_r+\nu\frac{\psi_r}{r}\right)\\
M_\theta&=B(r)\left(\frac{u_0}{r}+\nu u_{0,r}\right)+D(r)\left(\frac{\psi_r}{r}+\nu\psi_r,_r\right)\\
N_r&=A(r)\left(u_{0,r}+\nu\frac{u_0}{r}\right)+B(r)\left(\psi_r,_r+\nu\frac{\psi_r}{r}\right)\\
N_\theta&=A(r)\left(\frac{u_0}{r}+\nu u_{0,r}\right)+B(r)\left(\frac{\psi_r}{r}+\nu\psi_r,_r\right)\\
Q_r&=\frac{\kappa^2(1-\nu)}{2}A(r)(\psi_r+w,_r)
\end{aligned} \tag{11}$$

where

$$\begin{aligned}
A(r)&=\int_{-h/2}^{h/2}\frac{E}{1-\nu^2}dz=\bar{A}(g)\frac{E_c}{1-\nu^2}he^{\frac{r}{b}\mu}\\
B(r)&=\int_{-h/2}^{h/2}\frac{E}{1-\nu^2}zdz=\bar{B}(g)\frac{E_c}{1-\nu^2}h^2e^{\frac{r}{b}\mu}\\
D(r)&=\int_{-h/2}^{h/2}\frac{E}{1-\nu^2}z^2dz=\bar{D}(g)\frac{E_c}{1-\nu^2}h^3e^{\frac{r}{b}\mu}
\end{aligned} \tag{12}$$

To present a more general solution, the following non-dimensional parameters are introduced:

$$\bar{r}=\frac{r}{b},\quad \bar{w}=\frac{w}{b},\quad \tau=\frac{h}{b},\quad K_s=\frac{h^2k_s}{6D^*\kappa^2(1-\nu)},\quad K_w=\frac{k_wh^2b^2}{6D^*\kappa^2(1-\nu)} \tag{13}$$

where $D^* = E_c h^3 / 12(1-\nu^2)$ and K_w and K_s are the non-dimensional Winkler and Pasternak coefficients of the elastic foundation, respectively. Hereafter, the bar (-) symbol will not be shown for the sake of simplicity. Eqs. (8a) and (8c) may be simplified and rewritten based on Eqs. (11, 12) as:

$$\left(u_{0,rr}+\frac{u_{0,r}}{r}-\frac{u_0}{r^2}\right)\bar{A}(g)e^{\mu r}+\left(\psi_r{}_{,rr}+\frac{\psi_{r,r}}{r}-\frac{\psi_r}{r^2}\right)\bar{B}(g)\tau e^{\mu r}+\left(\psi_r{}_{,r}+\nu\frac{\psi_r}{r}\right)\bar{B}(g)\tau\mu e^{\mu r}$$
$$+\left(u_{0,r}+\nu\frac{u_0}{r}\right)\bar{A}(g)\mu e^{\mu r}=0 \tag{14a}$$

$$\left(u_{0,r}+\nu\frac{u_0}{r}\right)\bar{B}(g)\tau\mu e^{\mu r}+\left(\psi_r{}_{,r}+\nu\frac{\psi_r}{r}\right)\bar{D}(g)\tau^2\mu e^{\mu r}+\left(u_{0,rr}+\frac{u_{0,r}}{r}-\frac{u_0}{r^2}\right)\bar{B}(g)\tau e^{\mu r}$$
$$+\left(\psi_r{}_{,rr}+\frac{\psi_{r,r}}{r}-\frac{\psi_r}{r^2}\right)\bar{D}(g)\tau^2 e^{\mu r}-\frac{\kappa^2(1-\nu)}{2}(\psi_r+w_{,r})\bar{A}(g)e^{\mu r}=0 \tag{14b}$$

$$(\psi_{r,r}+w_{,rr})\bar{A}(g)e^{\mu r}+(\psi_r+w_{,r})\bar{A}(g)\mu e^{\mu r}+\frac{1}{r}(\psi_r+w_{,r})\bar{A}(g)e^{\mu r}$$
$$=\frac{h_0^2}{6D^*\kappa^2(1-\nu)}Pb+K_w(1+\alpha r+\beta r^2)w-K_s\left(w_{,rr}+\frac{1}{r}w_{,r}\right) \tag{14c}$$

3 BOUNDARY CONDITIONS

The most common edge conditions of the solid circular plates may be expressed as follows:

Roller-supported edge:

$$N_r=0,\quad M_r=0,\quad w=0 \tag{15a}$$

Immovable simply-supported edge:

$$u=0,\quad M_r=0,\quad w=0 \tag{15b}$$

Clamped edge:

$$u=0,\quad \psi_r=0,\quad w=0 \tag{15c}$$

4 SOLUTION PROCEDURE

Using Taylor's series expansion, the governing differential equations and the relevant boundary conditions of the system may be transformed into a set of algebraic equations in terms of the differential transforms of the original functions. Solution of these algebraic equations gives the desired solution of the problem.

Consider functions $u_0(r)$, $w(r)$, and $\psi(r)$ which are analytic in a domain R and let $r=r_0$ represent any point in R. These functions can be represented by power series whose center is located at $r=r_0$.

$$u_0(r)=\sum_{k=0}^{\infty}(r-r_0)^k U_k,\quad w(r)=\sum_{k=0}^{\infty}(r-r_0)^k W_k,\qquad \psi(r)=\sum_{k=0}^{\infty}(r-r_0)^k \chi_k \tag{16}$$

In practical applications, the function is usually expressed by a finite series. Therefore, Eq. (16) may be rewritten as

$$u_0(r)=\sum_{k=0}^{N}(r-r_0)^k U_k,\quad w(r)=\sum_{k=0}^{N}(r-r_0)^k W_k,\qquad \psi(r)=\sum_{k=0}^{N}(r-r_0)^k \chi_k \tag{17}$$

which implies that $u_0(r)=\sum_{k=N+1}^{\infty}(r-r_0)^k U_k$, $w(r)=\sum_{k=N+1}^{\infty}(r-r_0)^k W_k$, and $\psi(r)=\sum_{k=N+1}^{\infty}(r-r_0)^k \chi_k$ are negligibly small. In the present research, N is so chosen that the calculated stress components converge.

By substituting Eq. (17) into the governing Eq. (14), using Taylor's expansion for the exponential function around r_0=0, and performing some manipulations, the transformed form of Eq. (14) around r_0=0 may be obtained as:

$$\begin{aligned}&\sum_{k=0}^{N}\Big\{(1+\nu)\bar{A}(g)\mu U_{k+1}+\mu\bar{B}(g)\tau(k+1+\nu)\chi_{k+1}+(k+2+\nu)(k+1)\bar{A}(g)U_{k+2}\\&\quad+(k+2+\nu)(k+1)\bar{B}(g)\tau\chi_{k+2}+(1-\nu)(k+1)\bar{A}(g)U_{k+2}+(1-\nu)(k+1)\bar{B}(g)\tau\chi_{k+2}\Big\}r^k=0\end{aligned} \tag{18a}$$

$$\begin{aligned}&\sum_{k=0}^{N}\Big\{\mu\bar{B}(g)(k+1+\nu)U_{k+1}+\mu\bar{D}(g)\tau(k+1+\nu)\chi_{k+1}+\bar{B}(g)(k+1)(k+2+\nu)U_{k+2}\\&\quad+\bar{D}(g)\tau(k+1)(k+2+\nu)\chi_{k+2}+\bar{B}(g)(1-\nu)(k+1)U_{k+2}-\frac{\kappa^2(1-\nu)}{2\tau}(\chi_k+(k+1)W_{k+1})\bar{A}(g)\Big\}r^k=0\end{aligned} \tag{18b}$$

$$\begin{aligned}&\sum_{k=0}^{N}\Big\{\bar{A}(g)(k+2)(k+1)W_{k+2}+K_s(k+2)^2W_{k+2}+\bar{A}(g)\sum_{j=1}^{k}\frac{\mu^j}{j!}(k-j+2)(k-j+1)W_{k-j+2}\\&\quad+\bar{A}(g)\sum_{j=0}^{k}\frac{\mu^j}{j!}(k-j+1)\chi_{k-j+1}+\bar{A}(g)\mu\sum_{j=0}^{k}\frac{\mu^j}{j!}(k-j+1)W_{k-j+1}+\bar{A}(g)\mu\sum_{j=0}^{k}\frac{\mu^j}{j!}\chi_{k-j}\\&\quad+\bar{A}(g)\sum_{j=0}^{k}\frac{\mu^j}{j!}(k-j+2)W_{k-j+2}+\bar{A}(g)\sum_{j=0}^{k}\frac{\mu^j}{j!}\chi_{k-j+1}-\frac{K_w}{\tau}(W_k+\alpha W_{k-1}+\beta W_{k-2})\\&\quad-\frac{2(1+\nu)}{\kappa^2E_c}\frac{P_0}{\tau}(\lambda\delta(k-0)+\gamma\delta(k-1)+\xi\delta(k-2))\Big\}r^k=0\end{aligned} \tag{18c}$$

Simplifying Eqs. (18) and rearranging, the equations of motion can be rewritten as:

$$U_{k+2}=-\frac{1}{(k+3)(k+1)\bar{A}(g)}\Big\{\bar{B}(g)\tau(k+3)(k+1)\chi_{k+2}+(k+1+\nu)\bar{A}(g)\mu U_{k+1}\Big\} \tag{19a}$$

$$\begin{aligned}&\left(\bar{D}(g)-\frac{\bar{B}(g)^2}{\bar{A}(g)}\right)\tau(k+3)(k+1)\chi_{k+2}=\frac{\bar{B}(g)}{\bar{A}(g)}(k+1+\nu)\bar{A}(g)\mu U_{k+1}+\frac{\bar{B}(g)}{\bar{A}(g)}\mu\bar{B}(g)\tau(k+1+\nu)\chi_{k+1}\\&-\mu\bar{B}(g)(k+1+\nu)U_{k+1}-\mu\bar{D}(g)\tau(k+1+\nu)\chi_{k+1}+\frac{\kappa^2(1-\nu)}{2\tau}(\chi_k+(k+1)W_{k+1})\bar{A}(g)\end{aligned} \tag{19b}$$

$$\begin{aligned}&\left(\bar{A}(g)+\frac{K_s}{\tau}\right)(k+2)^2W_{k+2}=-\bar{A}(g)\sum_{j=1}^{k}\frac{\mu^j}{j!}(k-j+2)^2W_{k-j+2}-\bar{A}(g)\sum_{j=0}^{k}\Big\{\beta(k-j)(k-j-1)W_{k-j}\\&+\frac{\mu^j}{j!}\mu(k-j+1)W_{k-j+1}+(k-j+1)\chi_{k-j+1}+\mu\chi_{k-j}+\chi_{k-j+1}\Big\}+\frac{K_w}{\tau}(W_k+\alpha W_{k-1}+\beta W_{k-2})\\&+\frac{2(1+\nu)}{\kappa^2E_c}\frac{P_0}{\tau}(\delta(k-0)+\gamma\delta(k-1)+\xi\delta(k-2))\end{aligned} \tag{19c}$$

By substituting Eq. (17) into the boundary condition Eq. (15) the transformed form of Eq. (15) around r_0=0 will be:

Roller-supported edge:

$$M_r\big|_{r=1} = \bar{B}(g)\sum_{k=0}^{\infty}(k+\nu)U_k + \tau\bar{D}(g)\sum_{k=0}^{\infty}(k+\nu)\chi_k = 0,$$
$$N_r\big|_{r=1} = \bar{A}(g)\sum_{k=0}^{\infty}(k+\nu)U_k + \tau\bar{B}(g)\sum_{k=0}^{\infty}(k+\nu)\chi_k = 0, \tag{20a}$$
$$W\big|_{r=1} = \sum_{k=0}^{\infty}W_k = 0$$

Immovable simply-supported edge:

$$u\big|_{r=1} = \sum_{k=0}^{\infty}U_k = 0, \quad W\big|_{r=1} = \sum_{k=0}^{\infty}W_k = 0,$$
$$M_r\big|_{r=1} = \bar{B}(g)\sum_{k=0}^{\infty}(k+\nu)U_k + \tau\bar{D}(g)\sum_{k=0}^{\infty}(k+\nu)\chi_k = 0, \tag{20b}$$

Clamped edge:

$$u\big|_{r=1} = \sum_{k=0}^{\infty}U_k = 0, \quad w\big|_{r=1} = \sum_{k=0}^{\infty}W_k = 0, \quad \psi_r\big|_{r=1} = \sum_{k=0}^{\infty}\chi_k = 0, \tag{20c}$$

Based on Eq. (20), three boundary conditions are available along the plate edge (at r=1) that may be employed in solution of the Eq. (19) and consequently, determination of u_0, ψ , and w. Moreover, three additional conditions are required that may be extracted from the regularity conditions at the center of the moderately thick circular plate:

$$u\big|_{r=0} = 0 \quad \rightarrow U_0 = 0 \qquad \psi\big|_{r=0} = 0 \quad \rightarrow \chi_0 = 0 \qquad Q_r\big|_{r=0} = 0 \rightarrow W_1 = 0 \tag{21}$$

By substituting U_i, W_i and χ_i (i=2, ...,n+2) from Eq. (19) into Eq. (20) and applying the regularity conditions (21), the final system of equations will have the following form:

$$X_{11}^{(n)}U_1 + X_{12}^{(n)}W_0 + X_{13}^{(n)}\chi_1 = f_1, \quad X_{21}^{(n)}U_1 + X_{22}^{(n)}W_0 + X_{23}^{(n)}\chi_1 = f_2, \quad X_{31}^{(n)}U_1 + X_{32}^{(n)}W_0 + X_{33}^{(n)}\chi_1 = f_3 \tag{22}$$

U_1, W_0 and χ_1 may be determined by solving the mentioned system of equations. Other displacement parameters [U_i, W_i and χ_1 (i=2, ...,n+2)] may be determined based on the recursive Eq. (19).

5 TRANSVERSE SHEAR STRESS

It is evident that although the in-plane stresses may be determined accurately enough based on the first-order shear-deformation theory, the transverse stress components cannot be extracted directly from the constitutive equations. For this reason, we use the three-dimensional theory of elasticity to extract the transverse stress components based on variations of the in-plane stress components. Using equations of the three-dimensional theory of elasticity in terms of the stress components [20]:

$$\frac{\partial\sigma_r}{\partial r} + \frac{\sigma_r - \sigma_\theta}{r} + \frac{\partial\tau_{rz}}{\partial z} = 0 \tag{23}$$
$$\frac{1}{r}\frac{\partial(r\tau_{rz})}{\partial r} + \frac{\partial(\sigma_z)}{\partial z} = 0 \tag{24}$$

The transverse shear stress may be determined as:

$$\tau_{rz} = -\int_{-h/2}^{z}\left(\frac{\partial \sigma_r}{\partial r}+\frac{\sigma_r-\sigma_\theta}{r}\right)\mathrm{d}z$$
$$\tau_{rz} = -\int_{-h/2}^{z}\frac{E}{1-\nu^2}\left\{\frac{1}{b}\left[u_{0,rr}+\left(\mu+\frac{1}{r}\right)u_{0,r}+\left(\nu\mu-\frac{1}{r}\right)\frac{u_0}{r}\right]+\frac{z}{b^2}\left[\psi_r{}_{,rr}+\left(\mu+\frac{1}{r}\right)\psi_r{}_{,r}+\left(\nu\mu-\frac{1}{r}\right)\frac{\psi_r}{r}\right]\right\}\mathrm{d}z \quad (25)$$

or more precisely

$$\sigma_{rz} = -\frac{1}{b(1-\nu^2)}\left(u_{0,rr}+(\mu+\frac{1}{r})u_{0,r}+(\nu\mu-\frac{1}{r})\frac{u_0}{r}\right)\int_{-h/2}^{z}[(E_m-E_c)\left(\frac{1}{2}-\frac{z}{h}\right)^g+E_c]e^{\frac{r}{b}\mu}\mathrm{d}z$$
$$-\frac{1}{b^2(1-\nu^2)}\left(\psi_r{}_{,rr}+(\mu+\frac{1}{r})\psi_r{}_{,r}+(\nu\mu-\frac{1}{r})\frac{\psi_r}{r}\right)\int_{-h/2}^{z}[(E_m-E_c)\left(\frac{1}{2}-\frac{z}{h}\right)^g+E_c]e^{\frac{r}{b}\mu}z\mathrm{d}z \quad (26)$$

By substituting Eq. (26) into Eq. (24), the transverse normal stress component (σ_z) may be calculated:

$$\sigma_z = -\frac{1}{r}\int_{-h/2}^{z}\frac{\partial(r\tau_{rz})}{\partial r}\mathrm{d}z-\frac{P}{2} \quad (27)$$

6 RESULTS AND DISCUSSION

Example 1: To verify results of the present semi-analytical solution, a bending analysis example previously treated by Reddy et al. [21] and Nosier and Fallah [22], is reexamined. Both references used the first-order shear-deformation Mindlin plate theory, without elasticity corrections. The plate is assumed to carry a uniformly distributed transverse load. Although the edge of the plate is constrained, no elastic foundation is considered. Material and geometric parameters of the Titanium-Zirconia FGM plate are [21]: $E_m = 0.396E_c$, $\nu = 0.288$, $\tau = 0.2$.

It is evident that if the results are validated for the considered thick plate, higher accuracies will be expected for the moderately thick and thin plates. The following dimensionless maximum transverse deflection (that occurs at the center of the plate) is defined to extract the results: $\hat{w} = 64D^*w/Pb^4$. References [21] and [22] only considered plates made of transversely-graded materials $(\mu = 0)$ whereas in the present example, variations of the elasticity modulus in the radial direction is considered, too. Present results are listed in Table 1 and are compared with results of Refs. [21-22] for plates with clamped, simply-supported, or roller-supported edge condition, various volume fraction indices, and different thickness ratios. There is an excellent agreement among the results. As it may be expected, as the exponential exponent of the modulus of elasticity decreases, stiffness of sections adjacent to the constrained edge reduces and subsequently, the overall transverse deflection of the plate increases. On the other hand, as the edge movability increases, the overall deflection of the plate increases. Present results are almost coincident with results of the 3D elasticity.

Example 2: To perform a sensitivity analysis, a one-directional FGM plate with the following material and geometric specifications subjected to a no-uniform transverse load is considered [23]; $E_m = 200$ GPa, $E_c = 380$ GPa, $\nu = 0.3$, $g = 1$ and $\tau = 0.2$. As the foregoing example, the dimensionless maximum lateral deflection is defined as: $\hat{w} = 64D^*w/Pb^4$. Simultaneously, the results are compared with results of the 3D elasticity derived from the ABAQUS finite element model. In this regard, 20-noded brick elements are employed to model the plate. In the first stage of the sensitivity analysis, five loading conditions composed of: (i) uniform ($\lambda = 1, \gamma = 0, \xi = 0$), (ii) linear ($\lambda = 0, \gamma = 1, \xi = 0$ and $\lambda = 1, \gamma = 1, \xi = 0$), and (iii) parabolic ($\lambda = 0, \gamma = 0, \xi = 1$ and $\lambda = 1, \gamma = 0, \xi = 1$) distributions of the lateral load are considered to extract the results.

Table 1
Non-dimensional center deflections of FG circular plates under uniform transverse loads

Edge condition	g	Present study					Reddy et al. [21]	Nosier and Fallah [22]
		$\mu=-1$	$\mu=-0.5$	$\mu=0$	$\mu=0.5$	$\mu=1$	$\mu=0$	$\mu=0$
Clamped	0	5.5789	4.0801	2.9852	2.1852	1.6013	2.979	2.9792
	2	3.0173	2.2081	1.6163	1.1835	0.8671	1.613	1.6133
	10	2.4937	1.8247	1.3354	0.9777	0.7164	1.333	1.3330
	10^5	2.2092	1.6157	1.1821	0.8653	0.6341	1.180	1.1798
Simply-supported	0	17.6417	13.8203	10.828	8.46842	6.6001	10.822	10.8216
	2	9.31590	7.29402	5.7112	4.46420	3.47735	5.708	5.7083
	10	7.91130	6.19918	4.8575	3.79962	2.96154	4.855	4.8551
	10^5	6.98611	5.47285	4.2877	3.35349	2.61366	4.285	4.2854
Roller-supported	0	17.6417	13.8203	10.8276	8.46842	6.6001	10.822	10.8216
	2	9.64883	7.56282	5.9275	4.63756	3.61528	5.925	5.9247
	10	7.95251	6.23239	4.8843	3.82105	2.97859	4.882	4.8819
	10^5	6.98611	5.47285	4.2877	3.35349	2.61366	4.285	4.2854

Table 2
Non-dimensional center deflections of FG circular plates under non-uniform transverse loads

Edge condition	Approach	$\lambda=1$			$\lambda=0$	
		$\gamma=0,\xi=0$	$\gamma=1,\xi=0$	$\gamma=0,\xi=1$	$\gamma=1,\xi=0$	$\gamma=0,\xi=1$
Clamped	3D	1.580	2.262	1.942	0.682	0.362
	Analytical	1.596	2.282	1.958	0.685	0.361
	Difference (%)	1.04	0.88	0.83	0.51	0.07
Simply-Supported	3D	5.633	8.464	7.338	2.837	1.705
	Analytical	5.628	8.471	7.333	2.836	1.705
	Difference (%)	0.07	0.08	0.06	0.06	0.00
Roller-supported	3D	5.724	8.611	7.461	2.887	1.737
	Analytical	5.762	8.669	7.512	2.907	1.750
	Difference (%)	0.67	0.68	0.69	0.69	0.75

Table 3
Effects of the material heterogeneity exponents on the dimensionless lateral deflection of the plate for various thickness ratios and boundary conditions

Edge condition	τ	g=0			g=1			g=10		
		μ=-1	μ=0	μ=1	μ=-1	μ=0	μ=1	μ=-1	μ=0	μ=1
Clamped	0.05	3.544	1.922	1.036	2.525	1.369	0.742	2.063	1.119	0.603
	0.1	3.675	1.987	1.070	2.616	1.414	0.762	2.136	1.156	0.621
	0.15	3.894	2.099	1.128	2.765	1.490	0.801	2.257	1.215	0.653
	0.2	4.204	2.252	1.210	2.979	1.597	0.85۸	2.427	1.30	0.698
Simply-supported	0.05	12.521	7.763	4.771	8.717	5.401	3.315	7.270	4.510	2.771
	0.1	12.652	7.834	4.807	8.806	5.447	3.338	7.341	4.547	2.789
	0.15	12.873	7.942	4.862	8.954	5.521	3.377	7.462	4.605	2.819
	0.2	13.181	8.096	4.947	9.171	5.627	3.434	7.635	4.694	2.867
Roller-supported	0.05	12.521	7.763	4.771	8.922	5.534	3.399	7.296	4.525	2.779
	0.1	12.652	7.834	4.807	9.011	5.580	3.424	7.366	4.563	2.799
	0.15	12.873	7.942	4.862	9.158	5.652	3.463	7.488	4.621	2.829
	0.2	13.181	8.096	4.947	9.376	5.763	3.520	7.654	4.707	2.875

Results are given in Table 2 for various edge conditions and the differences between present results and results of the 3D theory of elasticity are calculated for the dimensionless lateral deflection of the center point of the plate. Although the plate is thick, there is an excellent agreement between the results. However, some researchers have proved that for relatively thin plates, accuracy of the results of the 3D theory of elasticity may be comparable to that of the plate theories [23-26]. As before, results of a plate with roller-supported edge are the greatest. In the second stage of the sensitivity analysis, effects of the transverse and radial material heterogeneity of a two-directional FGM plate on the dimensionless maximum lateral deflection are studied for thin, moderately thick, and thick plates. Results are shown in Table 3. These results reveal that influence of the radial heterogeneity on the maximum lateral deflection is significantly higher than that of the transverse heterogeneity. However, due to the adopted form of the dimensionless maximum lateral deflection expression, it seems that deflections of the thicker plates may be greater. Finally, effects of the elastic foundation and its radial stiffness distribution (uniform, linear, or parabolic distribution) on the dimensionless lateral deflection are evaluated. To this end, the following material and geometry information is used: g=1, μ=0.5 and τ=0.2.

Results given in Table 4 show that the edge conditions may affect results of the thick plates (τ=0.2) more than the elastic foundation, especially for edge conditions that led to higher rigidities. Furthermore, for identical stiffness values, in comparison with Winkler's foundation, Pasternak foundation (that exerts radial shear forces on the bottom surface of the plate) affects the results more remarkably.

Example 3: In the present example, displacement and stress distributions of transversely-graded FGM circular plates with simply-supported or clamped edges subjected to transverse loads are studied. To verify the results, especially the through-the-thickness distributions of the stress components, present results are compared with the 3D elasticity results obtained from ABAQUS. The following material and loading information is used:

$$E_m = 200 \text{ GPa},\ E_c = 380 \text{ GPa},\ g = 1,\ \frac{P_0}{E_c} = 1$$

Effects of the load function on the dimensionless lateral deflection $\hat{w} = 64D^* w / Pb^4$ are studied in Fig. 2. It is evident that the volume beneath the load distribution surface decreases when switching from the uniform to linear to parabolic load distributions, respectively. The through-the-thickness distributions of the radial bending and transverse shear stresses of simply-supported and clamped FGM plates subjected to a uniform transverse load (λ=1, P/E_c=1) are illustrated in Figs. 3 and 4, respectively (g=0, τ=0.2). Results are expressed based on the following dimensionless stress parameters: $\bar{\tau}_{rz} = \tau_{rz} / E_c$, $\bar{\sigma}_r = \sigma_r / E_c$. As it may be expected, the greatest transverse shear stresses occur in the neighborhood of the plate edge. Although the radial bending stress increases as one proceeds from the edge to the center of the simply-supported plate, a quite different trend is observed for the clamped plate. Indeed, sine the bending of the clamped plate so performs that an inflection point forms on any radial line connecting the edge to the center of the plate, the bending moment changes its sign in the radial direction and vice versa.

Table 4
Influences of the elastic foundation and its radial stiffness distribution on the dimensionless lateral deflection of the two-directional FGM circular plate

Edge condition	K_s	K_w=0.05			K_w=0.1			K_w=0.2		
		α=0, β=0	α=1, β=0	α=0, β=1	α=0, β=0	α=1, β=0	α=0, β=1	α=0, β=0	α=1, β=0	α=0, β=1
Clamped	0	1.112	1.095	1.105	1.061	1.028	1.046	0.9696	0.9165	0.9459
	0.05	0.8346	0.8243	0.8301	0.8045	0.7846	0.7962	0.7501	0.7168	0.7354
	0.1	0.6688	0.6618	0.6656	0.6490	0.6358	0.6432	0.6124	0.5898	0.6024
	0.2	0.4802	0.4765	0.4787	0.4699	0.4625	0.4665	0.4499	0.4369	0.4440
Simply-supported	0	3.690	3.456	3.567	3.171	2.841	2.995	2.471	2.090	2.262
	0.05	1.895	1.831	1.863	1.745	1.639	1.689	1.504	1.352	1.424
	0.1	1.268	1.239	1.253	1.198	1.147	1.172	1.078	0.9971	1.036
	0.2	0.7597	0.7488	0.7546	0.733	0.7136	0.7238	0.6854	0.6515	0.6682
Roller-supported	0	3.766	3.522	3.636	3.227	2.883	3.043	2.504	2.112	2.289
	0.05	1.915	1.849	1.881	1.762	1.653	1.704	1.516	1.362	1.435
	0.1	1.277	1.247	1.262	1.206	1.153	1.179	1.084	1.002	1.041
	0.2	0.7629	0.7520	0.7571	0.7360	0.7162	0.7264	0.6880	0.6541	0.6707

Effects of Winkler and Pasternak elastic foundations on reducing the radial bending and transverse shear stresses of the simply-supported plates (at r=0.9) are illustrated in Figs. 5 and 6, respectively. Comparing results shown in Figs. 5 and 6 confirms that Pasternak foundation reduces the resulting stresses more significantly. Results corresponding to the clamped plate are depicted in Figs. 7 and 8, respectively. These figures also confirm the previous conclusion.

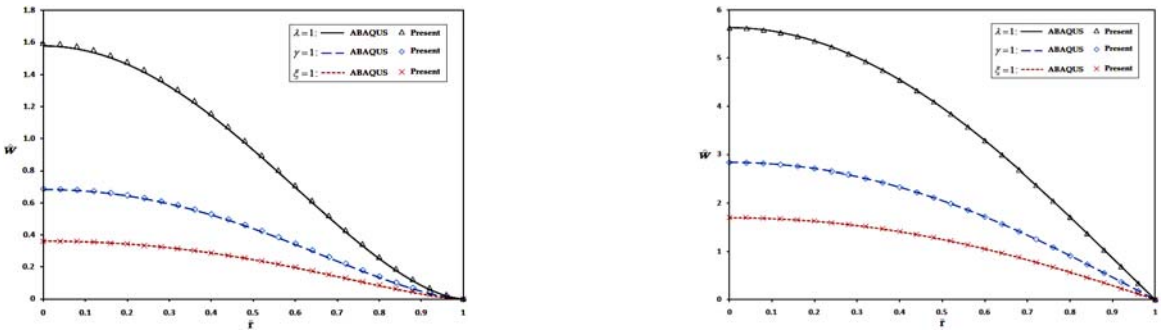

(a) (b)

Fig. 2
Radial distributions of the dimensionless lateral deflection of thick FGM (g=1, τ=0.2) circular plates with: (a) clamped and (b) simply-supported edges. Curves plotted with solid, dashed, and dotted lines correspond to uniform, purely linear, and purely parabolic distributions of the transverse load, respectively.

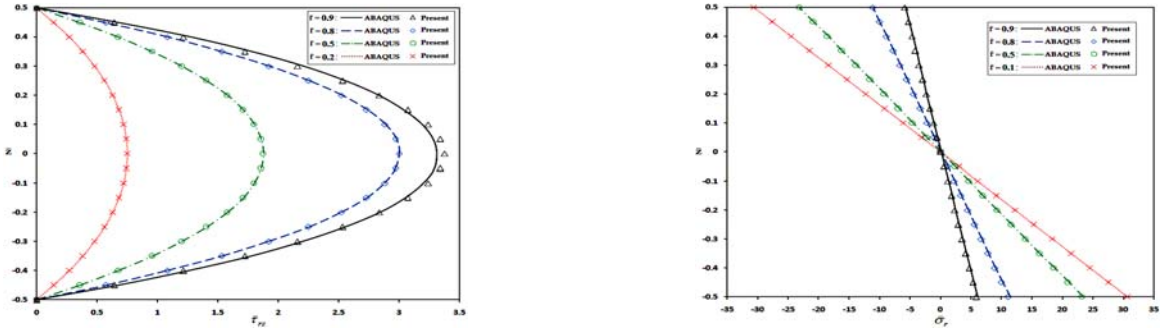

(a) (b)

Fig. 3
Through-the-thickness distributions of the radial bending and transverse shear stresses of a simply-supported FGM plate subjected to a uniform transverse load.

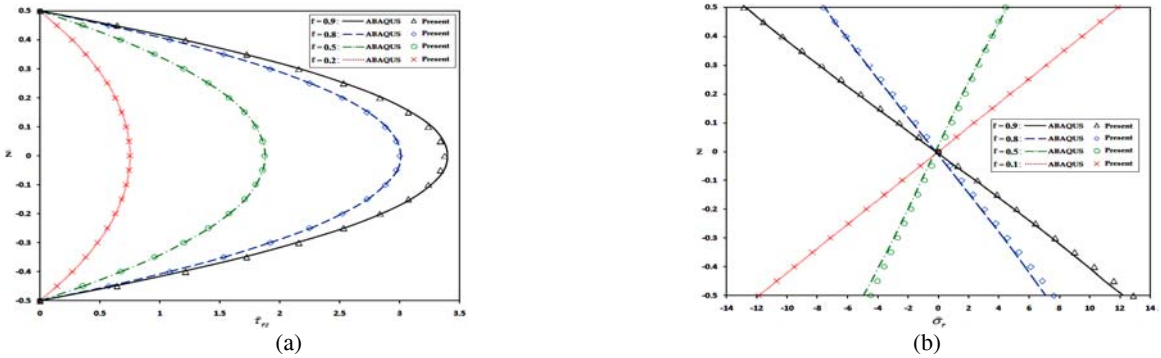

(a) (b)

Fig. 4
Through-the-thickness distributions of the radial bending and transverse shear stresses of a clamped FGM plate subjected to a uniform transverse load.

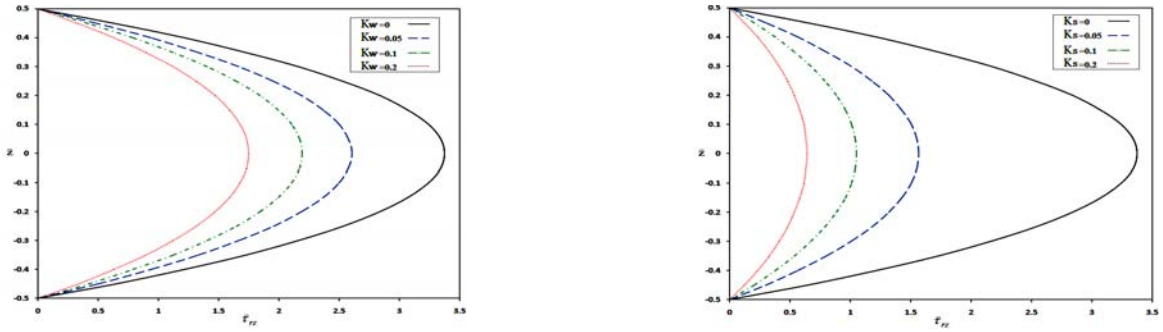

(a) (b)

Fig. 5
Effects of uniform: (a) Winkler and (b) Pastrenak stiffness coefficients of the foundation on the through-the-thickness distribution of the transverse shear stress of a simply-supported FGM plate subjected to a uniform transverse load, at r=0.9.

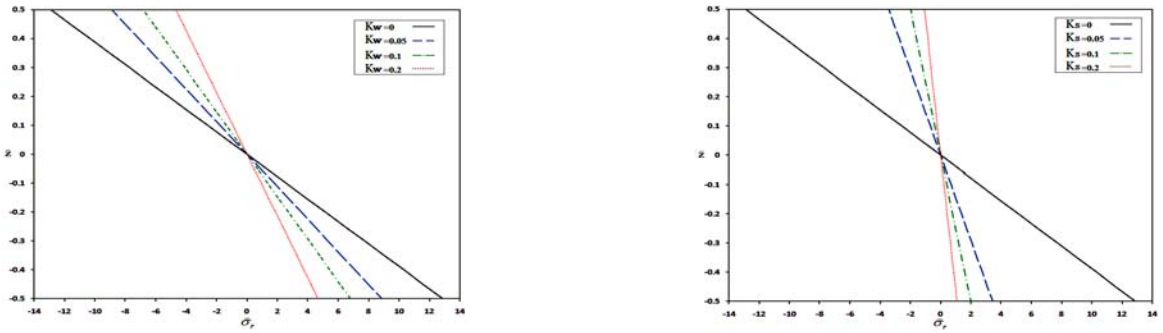

(a) (b)

Fig. 6
Effects of uniform: (a) Winkler and (b) Pastrenak stiffness coefficients of the foundation on the through-the-thickness distribution of the radial bending stress of a simply-supported FGM plate subjected to a uniform transverse load, at r=0.9.

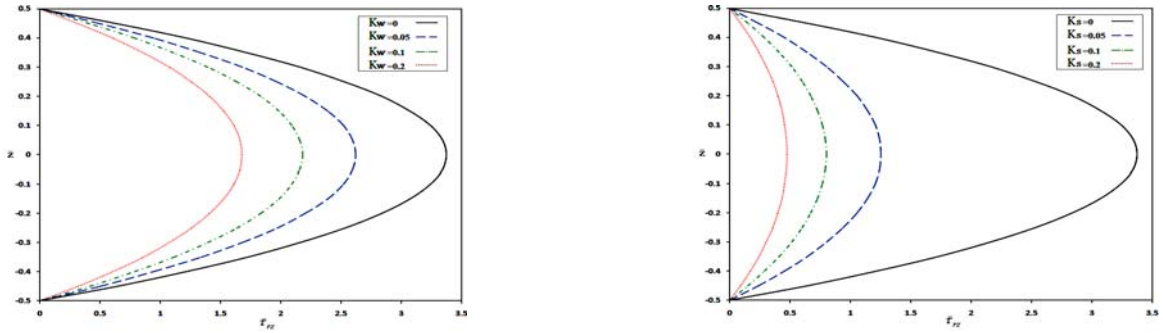

(a) (b)

Fig. 7
Effects of uniform: (a) Winkler and (b) Pastrenak stiffness coefficients of the foundation on the through-the-thickness distribution of the transverse shear stress of a clamped FGM plate subjected to a uniform transverse load, at r=0.9.

3D plots are presented for the dimensionless in-plane displacement $\hat{u} = 64D^* u / (Pb^4)$ distributions of the simply-supported and clamped plates in Fig. 9. Figs. 10 and 11 present 3D plots for the radial bending and transverse shear stresses of the simply-supported and clamped plates, respectively. Results are given for g=1 while other specifications are retained. Fig. 11 confirms that due to the sign change in the bending moment, signs of the bending stresses at r=0 and r=1 are opposite for each layer. However, due to using the 3D theory of elasticity, the transverse shear stress varies according to a somewhat parabolic function through the thickness.

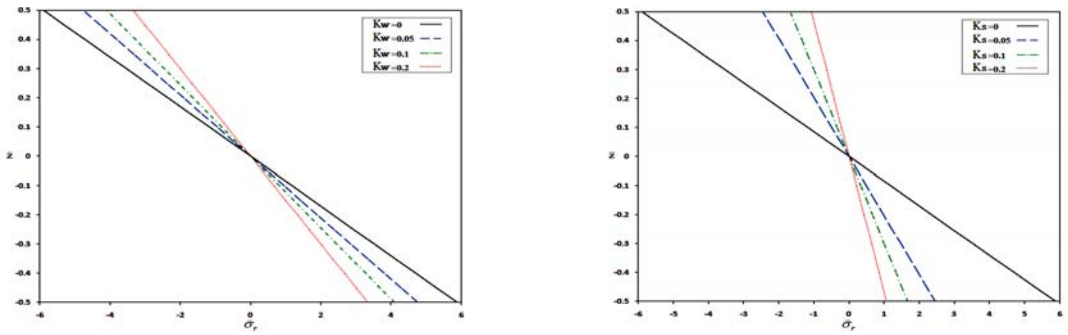

(a) (b)

Fig. 8
Effects of uniform: (a) Winkler and (b) Pastrenak stiffness coefficients of the foundation on the through-the-thickness distribution of the radial bending stress of a clamped FGM plate subjected to a uniform transverse load, at r=0.9.

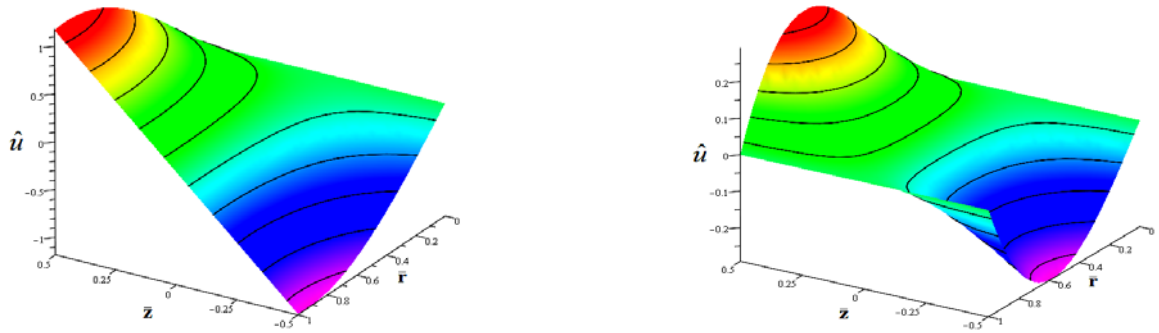

(a) (b)

Fig. 9
3D plots for the dimensionless in-plane displacement distribution for the: (a) simply-supported and (b) clamped plates.

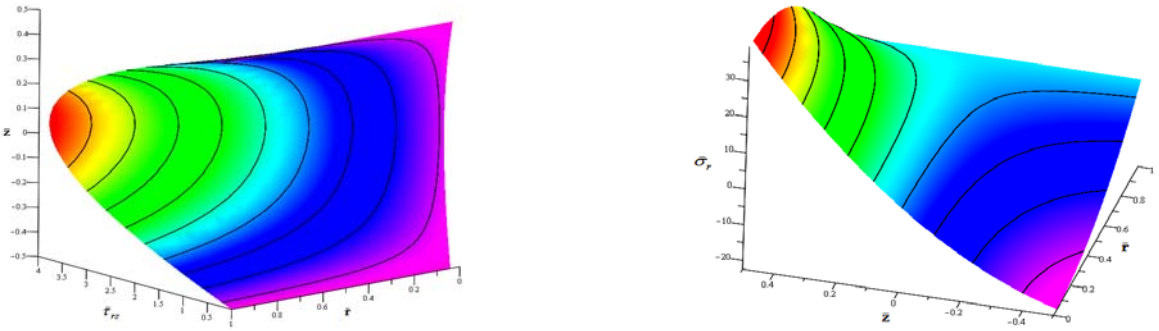

(a) (b)

Fig. 10
3D plots for the dimensionless radial bending and transverse shear stresses of the simply-supported FGM plate (g=1, τ=0.2, λ=1, P/E_c=1).

Fig. 12 illustrates effect of the volume fraction index of the clamped FGM circular plate on the through-the-thickness distribution of the dimensionless transverse normal stress $\bar{\sigma}_z = \sigma_z / E_c$. The stress is mainly affected by the externally applied loads and the foundation reaction. Hence the results which are not included here show a similar distribution for the simply-supported plate. Some researchers have reported that a monotonic increase in the volume fraction index may not lead to a unique pattern of variations in the results [27].

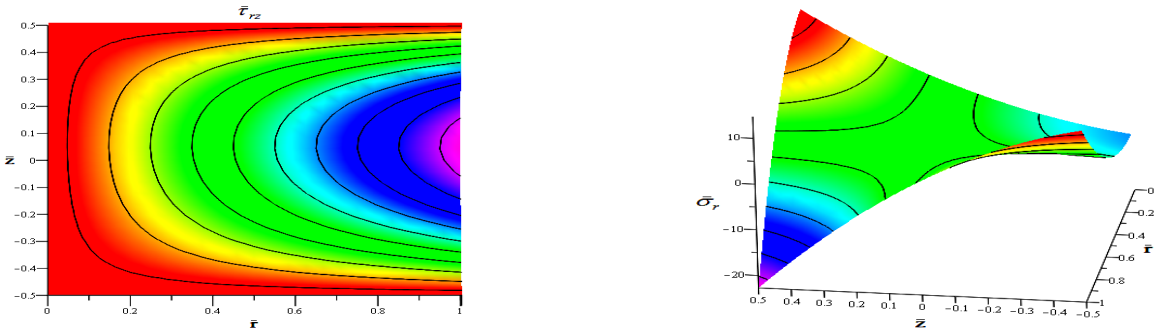

(a) (b)

Fig. 11
3D plots for the dimensionless radial bending and transverse shear stresses of the clamped FGM plate (g=1, τ=0.2, λ=1, P/E_c=1).

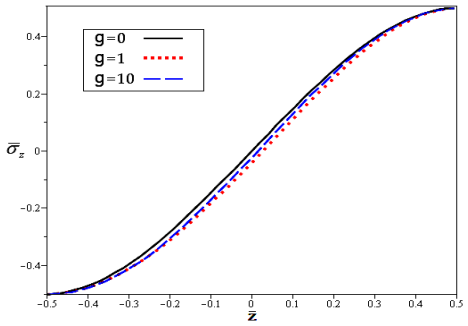

Fig. 12
Effect of the volume fraction index on the through-the-thickness distribution of the transverse normal stress of a clamped FGM circular plate.

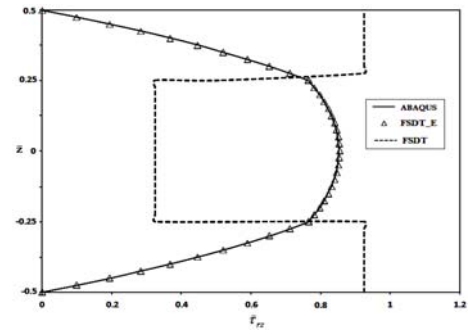

Fig. 13
Comparison of the present results for the through-the-thickness distribution of the transverse shear stress for a clamped three-layer sandwich plate (at r=0.5) with ABAQUS results and results of the traditional first-order shear-deformation theory.

Example 4: Finally, it is intended to prove that present approach may be extended and employed even for analysis of the sandwich plates. In other words, since a 3D elasticity correction is employed in the present paper for the transverse stresses, in contrast to the tradittional Mindlin theory that cannot satisfy the transverse stresses continuity at the interfaces between the layers, results of the present approach guarantee the mentioned continuity. To confirm this claim, a clamped three-layer (face sheet/core/face sheet) sandwich panel with the following material and geometry specifications is considered: E_1=E_3=200 GPa, E_2=70 GPa, τ_1=τ_3=0.1, τ_2=0.2. where the subscript *2* denotes the core. The through-the-thickness distribution of the dimensionless transverse shear stress predicted by the present approach (denoted by FSDT_E) is plotted in Fig. 13 for r=0.5 and compared with results of the 3D theory of elasticity (ABAQUS results) and results of the traditional constitutive-law-based first-order shear-deformation Mindlin theory (FSDT). Present results are almost coincident with results of the theory of elasticity. As Fig. 13 shows, in this case, results of the traditional first-order theory may not be reliable.

7 CONCLUSIONS

In the present paper, bending and stress analyses of two-directional functionally graded (FG) circular plates resting on non-uniform two-parameter foundations (Winkler-Pasternak foundations) is investigated using a semi-analytical solution. Some of the novelties of the present work are:

- Bending and stress analyses of the two-directional functionally graded circular plates are performed for the first time.
- The differential transform method (DTM) has not been used for stress analysis so far.
- The proposed semi-analytical solution is presented based on a first-order shear-deformation theory whose results are modified based on the 3D theory of elasticity.
- The presented solution is general and can be used for problems of two-directional heterogeneity, non-uniform transverse load, non-uniform stiffness distribution of the foundation, and various edge conditions.
- In contrast to the available first-order shear-deformation theories, present results are accurate enough, even for the thick plates.
- The proposed solution may be used for stress analysis of the sandwich plates, too. It guaranties continuity of the transverse stresses at the layer interfaces.

Results show that for identical values, in comparison with Winkler coefficient, Pasternak coefficient affects the results more remarkably and influence of the radial exponent of the modulus of elasticity is greater than that of the transverse exponent.

REFERENCES

[1] Reddy J.N., Wang C.M., Kitipornchai S., 1999, Axisymmetric bending of functionally graded circular and annular plates, *European Journal of Mechanics A/Solids* **18**: 185-199.

[2] Ma L.S., Wang T.J., 2004, Relationships between axisymmetric bending and buckling solutions of FGM circular plates based on third-order plate theory and classical plate theory, *International Journal of Solids and Structures* **41:** 85-101.

[3] Saidi A.R., Rasouli A., Sahraee S., 2009, Axisymmetric bending and buckling analysis of thick functionally graded circular plates using unconstrained third-order shear deformation plate theory, *Composite Structures* **89**: 110-119.

[4] Sahraee S., Saidi A.R., 2009, Axisymmetric bending analysis of thick functionally graded circular plates using fourth-order shear deformation theory, *European Journal of Mechanics A/Solids* **28**: 974-984.

[5] Jomehzadeh E., Saidi A.R., Atashipour S.R., 2009, An analytical approach for stress analysis of functionally graded annular sector plates, *Materials and Design* **30**: 3679-3685.

[6] Golmakani M.E., Kadkhodayan M., 2011, Nonlinear bending analysis of annular FGM plates using higher-order shear deformation plate theories, *Composite Structures* **93**: 973-982.

[7] Nie G., Zhong Z., 2007, Axisymmetric bending of two-directional functionally graded circular and annular plates, *Acta Mechanica Solida Sinica* **20**: 289-295.

[8] Li X.Y., Ding H.J., Chen W.Q., 2008, Elasticity solutions for a transversely isotropic functionally graded circular plate subject to an axisymmetric transverse load qr^k, *International Journal of Solids and Structures* **45**: 191-210.

[9] Li X.Y., Ding H.J., Chen W.Q., 2008, Three-dimensional analytical solution for functionally graded magneto–electro-elastic circular plates subjected to uniform load, *Composite Structures* **83**: 381-390.

[10] Yang B., Ding H.J., Chen W.Q., 2008, Elasticity solutions for a uniformly loaded annular plate of functionally graded materials, *Structural Engineering and Mechanics* **30**(4): 501-512.

[11] Lei Z., Zheng Z., 2009, Exact solution for axisymmetric bending of functionally graded circular plate, *Tsinghua Science and Technology* **14**: 64-68.

[12] Wang Y., Xu R.Q., Ding H.J., 2010, Three-dimensional solution of axisymmetric bending of functionally graded circular plates, *Composite Structures* **92**: 1683-1693.

[13] Nie G.J., Zhong Z., 2010, Dynamic analysis of multi-directional functionally graded annular plates, *Applied Mathematical Modelingl*. **34**(3): 608-616.

[14] Sepahi O., Forouzan M.R., Malekzadeh P., 2010, Large deflection analysis of thermo-mechanical loaded annular FGM plates on nonlinear elastic foundation via DQM, *Composite Structures* **92**(10): 2369-2378.

[15] Sburlati R., Bardella L., 2010, Three-dimensional elastic solutions for functionally graded circular plates, *European Journal of Mechanics A/Solids* 2011, dx.doi.org/10.1016/j.euromechsol.2010.12.008.

[16] Shariyat M., Alipour M.M., 2011, Differential transform vibration and modal stress analyses of circular plates made of two-directional functionally graded materials, resting on elastic foundations, *Archive of Applied Mechanics* **81**: 1289-1306**.**

[17] Alipour M.M., Shariyat M., Shaban M., 2010, A semi-analytical solution for free vibration of variable thickness two-directional-functionally graded plates on elastic foundations, *International Journal of Mechanics and Materials in Design* **6**(4): 293-304.

[18] Reddy J.N., 2007, *Theory and Analysis of Elastic Plates and shells*, Second Edition, CRC/Taylor and Francis, Philadelphia.

[19] Shen, H.-S., 2009, *Functionally Graded Materials: Nonlinear Analysis of Plates and Shells*, CRC Press, Taylor and Francis Group, Boca Raton.
[20] Ugural A.C., Fenster S.K, 2003, *Advanced Strength and Applied Elasticity*, Forth Edition, Prentice Hall, New Jersey.
[21] Reddy J.N., Wang C.M., Kitipornchai S., 1999, Axisymmetric bending of functionally graded circular and annular plates, *European Journal of Mechanics A/Solids* **18**: 185-199.
[22] Nosier A., Fallah F., 2008, Reformulation of Mindlin–Reissner governing equations of functionally graded circular plates, *Acta Mechanica* **198**: 209-233.
[23] Shariyat M., 2011, Non-linear dynamic thermo-mechanical buckling analysis of the imperfect laminated and sandwich cylindrical shells based on a global-local theory inherently suitable for non-linear analyses**,** *International Journal of Non-Linear Mechanics* **46**(1):253-271.
[24] Shariyat M., 2011, A double-superposition global-local theory for vibration and dynamic buckling analyses of viscoelastic composite/sandwich plates: A complex modulus approach, *Archive of Applied Mechanics* **81**: 1253-1268.
[25] Lezgy-Nazargah M., Shariyat M., Beheshti-Aval S.B., 2011, A refined high-order global-local theory for finite element bending and vibration analyses of the laminated composite beams, *Acta Mechanica* **217**: 219-242.
[26] Lezgy-Nazargah M., Beheshti-Aval S.B., Shariyat M., 2011, A refined mixed global-local finite element model for bending analysis of multi-layered rectangular composite beams with small widths, *Thin-Walled Structures* **49**: 351-362.
[27] Hosseini S.M., Sladek J., Sladek V., 2011, Meshless local Petrov–Galerkin method for coupled thermoelasticity analysis of afunctionally graded thick hollow cylinder, *Engineering Analysis with Boundary Elements.* **35**: 827-835.